Carbon 125 (2017) 336–343

Contents lists available at ScienceDirect

Carbon

journal homepage: www.elsevier.com/locate/carbon

# "Synthesis-on" and "synthesis-off" modes of carbon arc operation during synthesis of carbon nanotubes

Shurik Yatom [a, *], Rachel S. Selinsky [b], Bruce E. Koel [b], Yevgeny Raitses [a]

[a] Princeton Plasma Physics Laboratory, Princeton, NJ 08543, USA
[b] Department of Chemical and Biological Engineering, Princeton University, Princeton, NJ 08544, USA

ARTICLE INFO

*Article history:*
Received 1 August 2017
Received in revised form
1 September 2017
Accepted 9 September 2017
Available online 9 September 2017

ABSTRACT

Arc discharge synthesis of single-walled carbon nanotubes (SWCNTs) remains largely uncontrollable, due to incomplete understanding of the synthetic process itself. We show that synthesis of SWCNTs by a carbon arc may not constitute a single continuous process, but may instead consist of two distinct modes. One of these, a "synthesis-on" mode, produces the majority of the nanomaterials. During the synthesis-on mode, proportionally more carbon nanotubes are collected than in another mode, a "synthesis-off" mode. Both synthesis-on and synthesis-off modes for a typical arc configuration, employing a hollow anode filled with a mixture of powdered metal catalyst and graphite, were characterized by using in situ electrical, imaging, and spectroscopic diagnostics, along with ex situ imaging and spectroscopy. The synthesis-on mode duration is rare compared to the total arc run-time, helping to explain the poor selectivity found in the final collected products, a known inadequacy of arc synthesis. The rarity of the synthesis on mode occurence may be due to the synthesis off mode being more favorable energetically.


## 1. Introduction

Arc discharges are commonly used for the synthesis of nanomaterials, particularly high-quality single-walled carbon nanotubes (SWCNTs). The first nanotubes produced by arc discharge were reported by Ijima et al., in 1991 [1] and the number of studies of carbon nanotube (CNT) synthesis in arc conditions continues to grow [2,3]. A typical arc setup is relatively simple in both construction and implementation. It consists of two electrodes, one of which is consumed by ablation during the arc synthesis process. This electrode is typically a hollow graphite anode filled with a mixture of graphite and powdered metals, which provides the carbon and metal catalyst feedstock needed for SWCNT synthesis [2–6]. In spite of the simplicity of this design, it is commonly accepted that for CNTs, arc synthesis cannot match the selectivity, yield, and purity of other synthesis methods, e.g. chemical vapor deposition (CVD) and laser ablation. This belief arises in part from a small number of studies that have been performed investigating the fundamental physical and chemical mechanisms responsible for these limitations. The advantage of arc synthesis lies in the superior crystallinity of the synthesized CNTs, especially MWCNTs, where the nanotubes have less structural defects than those synthesized by using CVD. The discussion of ways and possibilities to optimize the conditions of arc assisted synthesis for nanotubes is ongoing [7].

The selectivity of the arc synthesis of SWCNTs is generally considered to be poor because a large fraction of the collected product is carbon soot and metal nanoparticles [5,6]. The most commonly collected product for SWCNT synthesis is the web-like material deposited on the chamber walls; however, Journet et al. [8] have found the "collar" formed around the cathode to be the richest in SWCNTs. In this work, we show that during arc operation synthesis occurs in an erratic fashion for undefined stretches of time. Further, we note that the arc plainly switches between two modes of operation: a dominant mode, where the discharge essentially happens between two solid graphite electrodes, and a much rarer mode involving the graphite powder and catalyst mixture. These two modes can be easily distinguished by using in situ diagnostics to monitor the arc dynamics and optical emission spectra. They are characterized by different emission spectra and different plasma characteristics. To the best of our knowledge no previous studies have reported that carbon arc synthesis is random and chaotic.

* Corresponding author.
*E-mail address:* syatom@pppl.gov (S. Yatom).

http://dx.doi.org/10.1016/j.carbon.2017.09.034
0008-6223/

## 2. Experimental

### 2.1. Carbon arc setup for SWCNT synthesis and witness plate system

The carbon arc setup used in these experiments has been described in detail elsewhere [9]. The electrodes are manufactured from single pieces of graphite and have diameters of 1.15 cm for the cathode and 0.60 cm for the anode. The anode is hollow with a cavity diameter of 0.275 cm. In this work, the anode is filled with a tightly pressed mixture of graphite powder and catalyst powder containing Ni and Y. The mixture weight ratio is 14:4.1:1 of graphite powder, Ni and Y (C–Ni–Y), respectively. We would like to note that the resistance of the solid graphite part of the anode and the resistance of the powder filling are very different. We have measured the resistances of both parts for currents ranging from 0.1-3 A, the resistance of the powder filling showed much higher values: several Ohms at low current and decreasing to ~1 Ohm for 3 A (due to heating), versus stable 0.15 Ohm of solid graphite. It resonable for the powder to ehxibit a higher resistance, because the contact between the particulates in the powder is not as good as in the solid structure. The electrodes are positioned vertically with the cathode located on top and the anode location controlled by a mechanical stepper motor. The chamber is evacuated to a fore-vacuum pressure and subsequently filled with He gas to a pressure of 500 Torr. The arc is ignited when the electrodes are in contact, and then they are separated to maintain a voltage of 27 V and a current of 60 A. Maximal arc run duration was up to 2 min, in order not to overheat the chamber. The fast framing imaging was performed with a Phantom V7.3 camera equipped with an optical filter at a central wavelength 470 nm and full-width-at-half-maximum (FWHM) of 10 nm. We employed a LeCroy WaveSurfer 10 oscilloscope (1 GHz, 10 Gs/s) and recorded the voltage with an active voltage divider and the current waveforms with a Pierson current monitor (model 4418). Optical emission spectra were recorded with an Ocean Optics HR2000+ spectrometer.

Samples of the carbon nanomaterials produced from the arc were collected during arc operation for ex situ analysis. The samples were collected on flat tantalum witness plates that were 5 cm long and 3 mm wide. At the start of the experiment, a witness plate was concealed inside a tantalum housing. The housing had a narrow slit through which the witness plate was manually deployed during arc operation. Deployment was affected via the rotation of a lever outside the chamber. The location of the witness plate deployment was chosen according to findings in Ref. [10], where the region of SWCNT growth was determined with a retractable probe. The process of shielding the witness plate and deploying it on demand allowed isolation of the products collected during the different arc operating modes and allowed for ex situ evaluation of the differences in nanomaterials produced during those modes.

### 2.2. Ex situ characterization and analysis

Nanomaterials deposited on the witness plates were analyzed using scanning electron microscopy (SEM), transmission electron microscopy (TEM), and Raman spectroscopy. The witness plates were qualitatively surveyed to identify the nanomaterial morphology and distribution on the plates using a FEI Verios 460 Extreme High Resolution Scanning Electron Microscope (XHR SEM). Elemental analysis was performed using an FEI Quanta 200 FEG Environmental-SEM equipped with Oxford X-Max 80 EDX and a ThermoFisher K-Alpha X-Ray Photoelectron Spectrometer (XPS/UPS). Samples for TEM were prepared by taking material from witness plates deployed during synthesis-off and synthesis-on modes, and then sonicating this material in ethanol using a conventional ultrasonic bath and then drop-casting the material onto lacey carbon grids. These grids were surveyed by using a FEI Talos F200× Scanning/Transmission Electron Microscope (S/TEM) to confirm that the CNTs being synthesized were SWCNTs. The witness plates were then analyzed directly using a Horiba LabRam ARAMIS Raman Spectrometer at 532 nm (2.33 eV) and 633 nm (1.96 eV).

## 3. Results and discussion

Previously we investigated the operation of a carbon arc with two solid electrodes under the same conditions, but without catalysts [9,11]. In these studies, the low [11] and high [9] frequency regimes of arc oscillations were observed and characterized. In the current setup using a graphite powder and catalyst mixture in the anode, we observed a correlation of the transition between these modes and changes in the sound produced by the arc. With the powder/catalyst-filled anode, the sound of the arc regularly transitions between a high-frequency hissing and a uniform low-frequency sound. Visual inspection showed that the hissing arc has oscillations, but when the sound transitions from hissing to uniform, the arc stabilizes. As soon as the arc is stable, the CNT-rich web starts to be formed in the volume and distributed throughout the chamber. Consequentially, we have designated the hissing operation as “synthesis-off” mode and the stable operation as “synthesis-on” mode.

### 3.1. In situ diagnostics

Arc behavior was studied using fast framing imaging of the discharge and the transition between the two discharge modes. Several frame rates were tested to record movies. The movies quickly validated that the transition in the sound could be used to distinguish between the different behaviors of the arc. Furthermore, we observed that in synthesis-off mode, the arc oscillated around the solid graphite component of the anode in a behavior analogous to that observed for solid anodes [9,11]. In synthesis-on mode, the oscillations disappeared and instead a strong jet appeared from the anode. Brief cycling between the modes, denoted as “spurting,” usually occurred for tens to hundreds of milliseconds before the system settled into continuous synthesis-on mode, which then persisted for tens of seconds.

#### 3.1.1. Fast framing imaging

Representative results of this spurting behavior are shown in Fig. 1, which is comprised of a set of still frames from a video of arc synthesis showing cycling between the two modes of synthesis. The images were taken through a 470 nm filter and so they emphasize emission from the Swan band of molecular $C_2$. The first five images show the low-frequency (~100 Hz) arc oscillations during the hissing mode. Images at $t = 4$ and 6 ms feature the anode spot that appears where the arc attaches to the outside of the anode during the low-frequency oscillations [11]. After eight milliseconds, stable emission in the form of diffuse jets originates from the anode cavity, which signifies the transition to the synthesis-on mode.

Supplementary video related to this article can be found at http://dx.doi.org/10.1016/j.carbon.2017.09.034.

In several frames ($t = 22–28$ ms), the jet emission is partially obstructed by an elongated black structure. This is likely a piece of the web material that has entered the region between the arc and the camera. After an additional period of 18 ms, the strong jet disappears and the arc goes back to the oscillating regime. Multiple arc runs, as subsequently viewed in the movies, provided the basis for a phenomenological explanation of the two synthesis modes, as shown schematically in Fig. 2. The synthesis-off mode occurs when the anode is partially empty, i.e. when the level of powdered

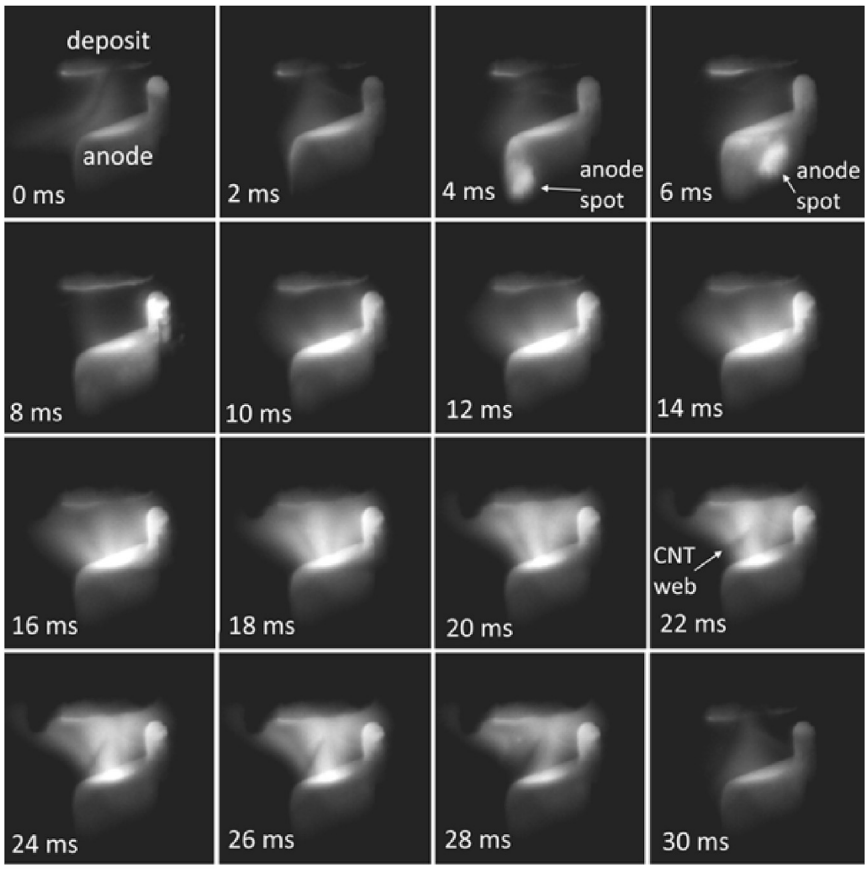


**Fig. 1.** Transitions between synthesis-on and synthesis-off modes. In this series of images, the synthesis-on mode begins at 10 ms and ends at 30 ms. In the third and fourth frames, (4 and 6 ms, respectively), the anode spot, i.e. the location where the arc is attached to the anode surface, is labeled, showing that the arc is attached to the outside of the anode in these two frames.

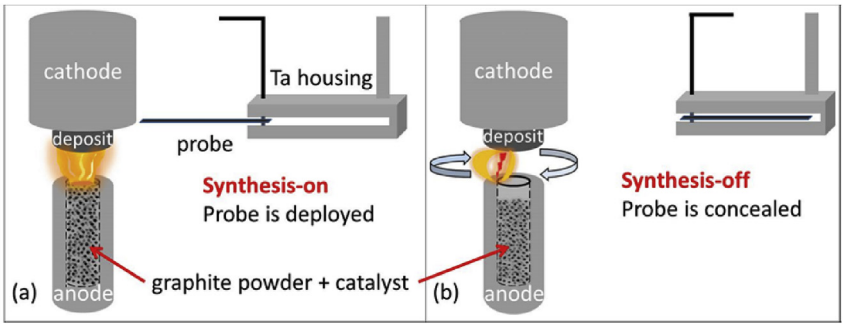


**Fig. 2.** Transitions between synthesis-on and synthesis-off modes and schematics of witness plate deployment and concealment. (a) Synthesis-on regime: Arc engages the graphite and catalyst powder, and it proceeds to a stable synthesis-on mode that no longer oscillates and is characterized by much more intensive $C_2$ emission. The witness plate is deployed when the mode has stabilized. (b) Synthesis-off regime: Arc oscillates around the surface of the hollow anode and is unable to interact with C–N–Y mixture that was depleted from the top part of the anode. The witness plate is concealed when the arc is in the synthesis-off mode. (A colour version of this figure can be viewed online).

graphite and metal in its core is several millimeters below the tip of the solid graphite. This mode is characterized by arc oscillations, with a behavior identical to that of arcs run with solid graphite anodes (containing no catalyst). During the synthesis-off mode, the arc oscillations slowly ablate the solid graphite component until its level approaches the level of the powder/catalyst mixture in its core.

As the fresh powder/catalyst mixture is exposed to the arc, a rapid cycling between synthesis-on and synthesis-off modes begins. The oscillating arc (synthesis-off mode) engages the powder mixture for short periods of time causing short bursts of intense light indicative of “spurts” (short periods of the synthesis-on mode). Each such spurt appears as a jet from the anode cavity towards the cathode deposit. After a series of these spurts, the arc settles into a continuous synthesis-on mode that persists for seconds to tens of seconds. As soon as the powder mixture at the top of the anode is depleted, the characteristic oscillating behavior analogous to that of a solid graphite anode resumes, indicating a return to the synthesis-off mode. Cycling of the arc between these two modes continues until the powder is fully depleted or the arc stops.

### 3.1.2. Electrical measurements

The transition between the arc synthesis modes is also evident in the voltage and current waveforms, as shown in Fig. 3. Brief mode changes or spurts manifest in the voltage waveform as rapid increases of the voltage from 27 to 40 V and rapid decreases back to 27 V. In the continuous synthesis-on case, the voltage also increases to 40 V and then slowly lowers to a 32–34 V level. Fig. 3 shows that the voltage jumps from 33 to 48 V just before the end of the continuous synthesis-on mode. Current oscillations also correlate with the voltage; however, the amplitude of these oscillations is very low, which is quite reasonable when operating with a constant current power source. Why does the voltage undergo such a dramatic increase? A voltage rise during constant current means that, according to Ohm's law, there must have been a surge in resistance. In the case of arc synthesis, the resistance increases due to a combination of two factors: plasma losses to micron sized graphite particles, and increased electron-neutral collisions. Graphite particles are the majority component of the anode powder filling and range in size between 5 and 10 μm. Plasma losses associated with the graphite particles are akin to wall losses, where electrons diffuse and are lost at the chamber walls. Injection of many large particles into the discharge gap effectively increases the wall area, and thus this injection prevents a significant portion of the electrons from reaching the anode. The graphite micro-particles also sublime in the hot region of the plasma channel and this results in the disintegration of graphite into carbon molecules and atoms. This surge in neutral density boosts the electron-neutral collision rate and accordingly raises the plasma resistance. Either of these mechanisms could be responsible for the observed change in voltage; however in the arc conditions studied herein, the change likely results from a combination of both mechanisms. Additionally, one may consider the higher resistance of the powder filled part. As mentioned above, the observed voltage jumps between the modes are 6-13 V and at current of 60 A these are explained by the resistance difference of 0.1-0.21 Ohm. Furthermore, this may also explain that the voltage jumps to 40 V at the very onset of the synthesis on and then decreases as current heats the filling and its resistance subsequently lowers.

### 3.1.3. Optical emission spectroscopy

The emission spectrum from the arc could reasonably be expected to change significantly between the synthesis-on and synthesis-off modes, because the imaging and electrical characteristics of the plasma in these modes are observed to be drastically different. Indeed, a survey of the broadband optical emission shows that in the synthesis-off mode the only prominent features are the Swan bands corresponding to the emission of $C_2$ and the blackbody emission of the hot electrodes and plasma.

When the synthesis-on mode starts the emission from the Swan bands intensifies and emission from the metals emerges. Most of the time this emission consists of that from Y and Ni neutrals; however, for brief periods of time the emission is augmented by multiple Y ion lines and a single Ni ion line. Because these lines only appear for a short duration, we attribute them to the spurting behavior observed during the transitions between modes. The described emission patterns are shown in Fig. 4. This is crucial evidence that most of the synthesis of SWCNTs occurs during the synthesis-on mode, because metal catalysts are essential for the formation of SWCNTs [3,5,6].

### 3.1.4. A case for universality: electrical current

While 60 A is commonly chosen for running arc-assisted synthesis experiments, other currents are also used, and therefore we also performed our experiment at a current of 100 A to verify our findings. We observed both synthesis-on and synthesis-off modes for 100 A current, confirming that this is not a unique phenomenon for 60 A current operation. The main difference between the two current cases is that, when employing 100 A current, we were not able to obtain continuous synthesis-on mode behavior, i.e. the synthesis-on mode was only observed in spurts spaced by ~30–60 ms periods of oscillations in the synthesis-off mode. The FWHM of a spurt was determined to be > 10 ms. Since the spurts are very short, they are not distinguishable when observing the discharge with the naked eye, unlike the visible continuous synthesis-on mode for 60 A current operation. At 100 A, spurts do not generate a distinctive sound, but seem akin to the continuous synthesis-on mode behavior. However, the spurts are still easily observed through fast

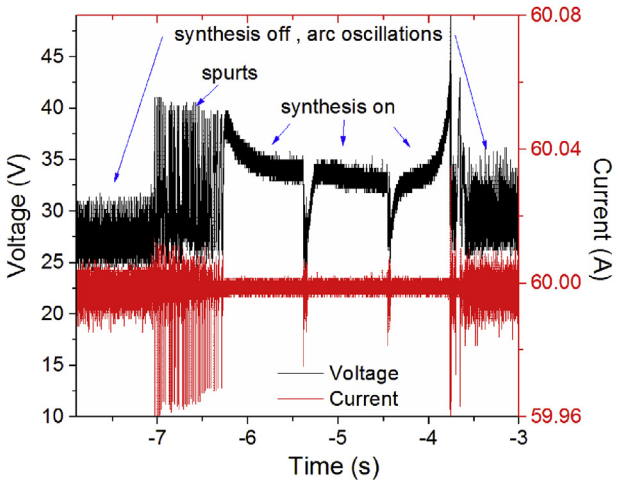


**Fig. 3.** Voltage and current waveforms bearing evidence of the transitions between modes. The voltage increases rapidly when the synthesis starts and a period of short pulses (spurts) of synthesis-on mode follows. The voltage slowly decreases during the continuous period of the synthesis-on mode, but still remains significantly higher than during the synthesis-off mode. (A colour version of this figure can be viewed online).

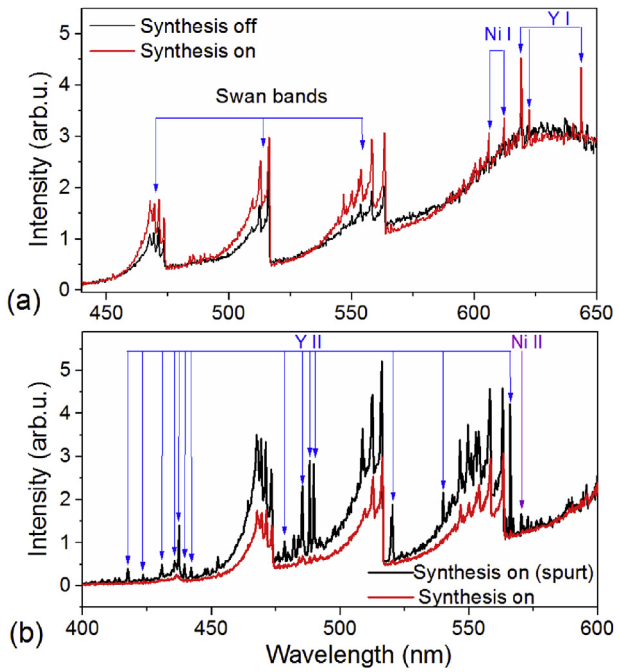


**Fig. 4.** (a) Emission in synthesis-off and synthesis-on modes. (b) Occurrence of metal ions lines during a spurt of the synthesis-on mode and more stable synthesis-on mode. (A colour version of this figure can be viewed online).

framing imaging and voltage waveforms, in which the voltage increases quickly from 27 to 38–40 V, as in the 60 A case shown in Fig. 3. Periods of continuous synthesis-off oscillations were also observed, which lasted for 2–3 ms without interruption by spurts.

*3.1.5. A case for universality: effect of the anode hole diameter*

In the long history of arc-assisted synthesis a variety of anode hole diameters from 2.5 to 4 mm were employed, while the total diameter of the anode remained at 0.6–0.65 cm in most experiments. We have conducted a check of whether or not the diameter of the anode hole influences the mode transition. To that end, we have operated the arc using anodes with holes of 0.4 cm diameter, in addition to the 0.275 cm diameter holes that we have generally used. All anodes were manufactured from the same material, and the arc current for all experiments was set at 60 A. The experiments were done to check the behavior qualitatively, and no quantitative data was collected for these additional anodes. The discharge behavior was monitored using a fast framing camera and voltage sensors. For a 0.4 cm diameter hole, the transition between the modes was easily observed. The continuous synthesis-on mode appeared more frequently and for longer durations. The consumption of the anode walls was much faster for a 0.4 cm diameter hole than for a 0.275 cm hole, allowing for more frequent contact of the arc plasma with the catalyst-containing powder. The downside of operating with such an anode is the enhanced ablation rate. In order to maintain the same arc conditions, the gap between the electrodes is kept very small ($\geq$1 mm) throughout the discharge. As a result, less product is generated in the volume (significantly less web is observed in the chamber) and more product is formed as part of the cathode deposit. Since the main goal of carbon arc synthesis is SWCNT production in volume, lower operating currents may be required to mitigate this shortcoming and allow for a larger inter-electrode gap. Despite these observations, the larger hole diameter clearly does provide longer, more stable, and more frequent operation in a synthesis-on mode, though caveats remain in terms of product generation and collection. This confirms that the phenomenon of mode transition persists for a representative range of holes diameters.

*3.1.6. Ablation rate of synthesis-on and synthesis-off modes*

In the fast-framing imaging experiments, we have observed that the deposit growth rate is vastly dissimilar between the two arc modes, which is most likely evidence of different ablation rates of the anode during the two modes. The ablation rate of the anode is of interest for identifying the ablation regime and for comparing findings to the solid graphite anode case [12,13]. There are no reports available in the literature of the anode ablation rate for experiments using anodes filled with a graphite powder and catalyst mixture. Consequently, we have measured the ablation rate of the anode during our experiments. The measurements included weighing both the anode and cathode before and after the experiment, so that the weight lost by the anode and the weight gained by the cathode could be determined. Since the arc operation transitions between the two aforementioned modes, we have used voltage waveforms and the fast-framing video clips in order to calculate the duration that the arc spent in each mode during the run. The goal was to evaluate the ablation rate in the synthesis-on and synthesis-off modes separately. For each analyzed run, we solved for two unknowns, which were the synthesis-on ablation rate and the synthesis-off ablation rate. Knowing the time spent in each mode and the total weight lost by the anode allows one to determine the two unknowns after two separate measurements. We found the ablation rates to be $3.5 \pm 1.1$ mg/s and $15.6 \pm 0.8$ mg/s, in synthesis-off and synthesis-on modes, respectively. These calculated rates are the average ablation rates for each mode over the course of the analyzed run. The ablation rate at any given moment during a run depends on the length of the inter-electrode gap, and this distance depends on the topography of the anode surface that changes notably between and within arc runs. Likewise, the ablation rates change with current and anode hole diameter, so these results are not standard for every carbon arc experiment, but nevertheless serve to illustrate the contrast between the two arc regimes.

Furthermore, the difference in the weight gained by the cathode and the weight lost by the anode enables us to calculate an upper limit for the amount of ablated carbon that is free to participate in the synthesis of SWCNTs and other structures in the volume. The analysis of several measurements indicates that 57% of the material ablated from the anode ends up as cathode deposits, and so 42% of the ablation material from the anode can take part in volume synthesis of nanomaterials.

*3.1.7. Frequency of the synthesis-on mode*

A supplementary analysis was carried out to determine which mode dominates the anode lifetime. To this end, we analyzed the duration of each mode for 5 identical anodes. For each anode, the total duration of synthesis-on and synthesis-off modes was determined from inspection of the voltage waveforms. Synthesis-on duration time includes both short spurts and the continuous synthesis-on condition. The ratio of synthesis-on time to total anode lifetime was calculated as the percentage of total anode lifetime that was spent in the synthesis-on regime. The results for the five analyzed anodes were 8.4, 12.7, 14, 16, and 21%. This spread of values is likely due to the fact that anode topography changes drastically during the discharge and thus impacts the ablation rate and total lifetime. However, this result clearly shows that the arc predominantly operates in the synthesis-off mode.

In spite of the fact that a similar full analysis was not conducted for discharge currents of 100 A, one can make a similar qualitative claim for 100 A operation. As mentioned earlier for the case of 100 A, the synthesis-on mode appears exclusively in spurts with a FWHM of >10 ms, spaced by 30–60 ms of synthesis-off mode oscillations. Also, an exclusively synthesis-off regime (without spurts) was observed for durations up to 2–3 s. Therefore, we conclude that the dominance of the synthesis-off mode during the anode's lifetime also extends to the 100 A regime.

*3.2. Ex situ characterization*

The in situ visual and spectroscopic observations of the plasma during synthesis-off and synthesis-on modes were compared to ex situ characterization of the nanomaterials produced. SEM and TEM imaging were employed to identify the types of nanomaterials collected during the separate synthesis modes, and Raman spectroscopy was used to provide a qualitative indication of selectivity.

*3.2.1. Electron microscopy*

Visually, the witness plate exposed during the synthesis-off mode collected far less material than the plate exposed during the synthesis-on mode, and this observation was further confirmed by SEM characterization. The plates were examined by SEM at intervals of 1 mm starting at the end presented to the plasma. For both samples, the largest quantity of materials was collected at the end nearest to the plasma, and the amount of material decreased with increased distance from the plasma. The witness plates used in these experiments were not inserted into the interstitial space between the electrodes, and so the observed distribution of collected materials is consistent with another report in the literature [14]. The material collected on the synthesis-on plate was more plentiful and extended much further than did the material on

the synthesis-off plate. For both the synthesis-off and synthesis-on samples, the primary morphology observed appeared to be spherical soot, as seen in the representative images shown in Fig. 5. The samples collected during both synthesis-off (5a) and synthesis-on (5b) modes contained SWCNTs; however, during the synthesis-on mode far more material was collected and the ratio of SWCNTs to soot was much higher. This result supports the hypothesis that SWCNTs are produced primarily during the synthesis-on mode. While the SWCNTs collected during the synthesis-off mode may have been grown during the synthesis-off regime, there are other explanations possible for the presence of trace amounts of SWCNTs. These SWCNTs may have been grown during the synthesis-on mode, but were still circulating in the atmosphere of the chamber (having not yet been deposited on the walls) when the synthesis-off mode commenced. Alternatively, the SWCNTs may have been formed during the rare spurts of synthesis-on mode behavior that have been observed to occur during otherwise continuous synthesis-off mode operation.

Samples taken from the synthesis-off and synthesis-on witness plates were then examined by TEM and this confirmed that the CNTs were single-walled. In the synthesis-off mode case, very few SWCNTs were observed and those that were seen were isolated (Fig. 5c). In the synthesis-on mode case, a high proportion of the nanomaterials observed were high quality SWCNTs and they were frequently seen in bundles (Fig. 5d). In addition to SWCNTs, the spherical soot observed by SEM for both synthesis-off and synthesis-on conditions was determined by TEM to be comprised of single-walled carbon nanohorns (SWCNHs).

Elemental analysis was performed on the witness plates by both EDX and XPS to study the ratio of metal catalyst (Ni and Y) to carbon collected during each synthesis mode. For both EDX and XPS, Ni and Y were detected on the synthesis-off and synthesis-on witness plates; however, in all cases, the quantities observed were insufficient for meaningful quantification.

### 3.2.2. Raman spectroscopy

Raman analysis was performed on samples taken during both synthesis-off and synthesis-on modes to confirm the presence of SWCNTs. These spectra confirm our observations made by SEM and TEM, showing the presence of SWCNTs, SWCNHs, and amorphous carbon [14–16]. The most reliable indicator of the presence of SWCNTs is the observation of the radial breathing mode (RBM) features. The RBM frequency ($\omega_{RBM}$) corresponds to the coherent radial vibrations of carbon atoms and these occur in the range of 120–350 $cm^{-1}$ [14]. RBM features were observed for both synthesis-on and synthesis-off samples, which was an expected result given the SEM and TEM analyses. Additional characteristic vibrations of SWCNTs include: a pair of strong sharp peaks at 1563 and 1587 $cm^{-1}$ corresponding to the $G^-$ and $G^+$ modes, respectively; a weak, broad peak at 1324 $cm^{-1}$ corresponding to the D mode; and weak peaks at 1614, 1729, 1750, 1962, ~2675, 2900, and 3180 $cm^{-1}$ corresponding to the D′, $M^-$, $M^+$, iTOLA, G′, 2LO, and 2G modes, respectively [14]. A comparison of spectra obtained for materials deposited during synthesis-off and synthesis-on modes with all of these peaks labeled can be seen in Fig. 6a, where the spectra are normalized to the D mode intensity. SWCNHs are structurally similar to SWCNTs and have two broad, relatively weak peaks of approximately equal height corresponding to the D and G modes at the same frequencies that are seen for SWCNTs [14,15]. A broad feature at 1538 $cm^{-1}$ corresponds to amorphous carbon (a-C) [16].

Contributions by the aforementioned nanomaterials to the measured Raman spectra of samples obtained during synthesis-off and synthesis-on modes were determined by curve fitting using the characteristic modes. A fifth-order polynomial baseline correction was applied, and the peaks due to D, $G^-$, $G^+$, D′, $M^-$, $M^+$, and iTOLA modes of SWCNTs and the peak associated with amorphous carbon were fitted with Lorentzian lineshapes [14]. The fits for D, a-C, $G^-$, $G^+$, and D′ contributions are shown in Fig. 6b and c. The D and G peaks of SWCNHs are subsumed by the D and G peaks of SWCNTs and so the final heights of these fits have contributions from both types of materials.

To determine the effect of the arc operation modes on the selectivity for producing SWCNTs versus SWCNHs, we considered the ratio of the $G^+$ peak intensity (which comes predominantly from SWCNTs with a small contribution from SWCNHs) to the D peak intensity (which is expected to have similar contributions from both SWCNHs and SWCNTs). As the fraction of SWCNTs in the sample increases relative to SWCNHs, this ratio should also increase. This ratio was 3:2 for the sample collected during synthesis-off mode and 9:2 for the sample collected during synthesis-on mode. This qualitatively confirms that there is a higher ratio of

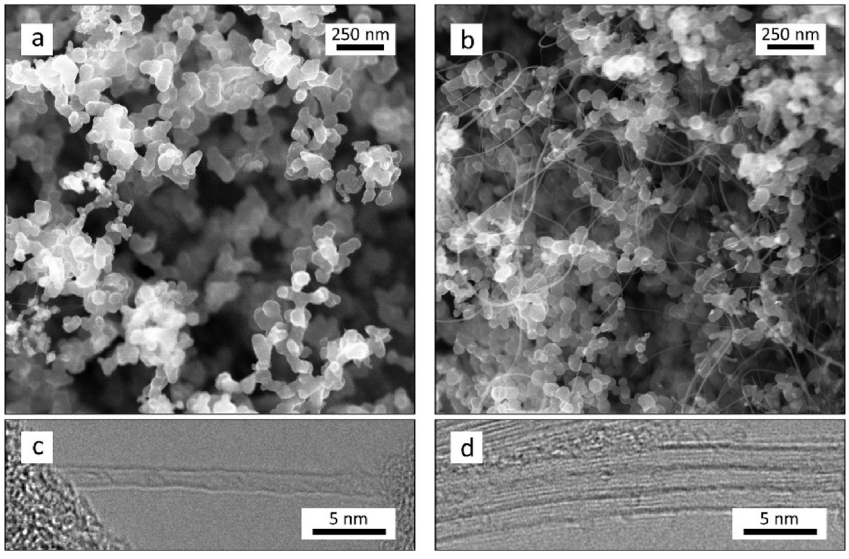


**Fig. 5.** Representative (top) SEM and (bottom) TEM images of the nanomaterials captured by witness plates exposed during (a, c) synthesis-off and (b, d) synthesis-on modes.

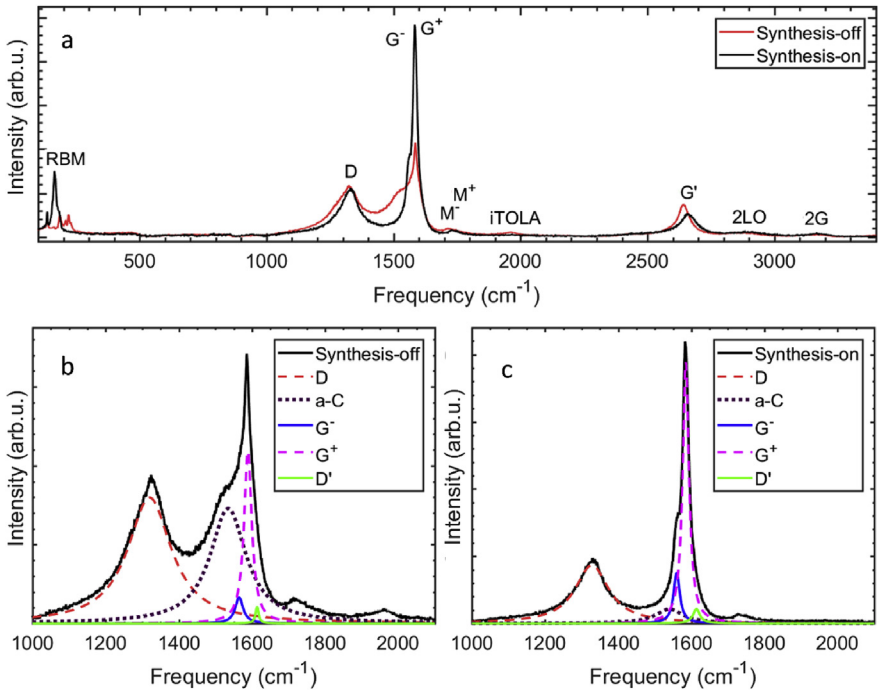


**Fig. 6.** Raman spectra of nanomaterials produced during synthesis-off and synthesis-on modes. (a) Comparison of spectra (normalized to the D peak intensity) of materials obtained during synthesis-off and synthesis-on modes with the characteristic vibrational peaks labeled. (b,c) Expanded view showing the spectral fits of key vibrational peaks used for comparing the products from operation in synthesis-off and synthesis-on modes, respectively. (A colour version of this figure can be viewed online).

SWCNTs to SWCNHs produced during synthesis-on compared to synthesis-off mode operation. To determine the effect of the arc modes on the selectivity for SWCNTs versus amorphous carbon, we considered the ratio of the $G^+$ peak intensity (which comes predominantly from SWCNTs with a small contribution from SWCNHs) to the intensity of the peak associated with amorphous carbon. As the fraction of SWCNTs in the sample increases with respect to amorphous carbon, this ratio should increase. This $G^+$/a-C ratio was 3:2 for the sample collected during synthesis-off mode and 36:2 for the sample collected during synthesis-on mode. This qualitatively confirms that there is a higher ratio of SWCNTs to SWCNHs produced during the synthesis-on mode than during the synthesis-off mode.

## 4. Conclusions

The results described herein reveal that operation of a carbon arc for carbon nanomaterials synthesis switches between two modes: a dominant “synthesis-off” mode, where the discharge essentially happens between two solid graphite electrodes and produces little if any nanomaterials in volume, and a much rarer “synthesis-on” mode involving a discharge between a graphite cathode and a mixture of powdered metal catalyst and graphite in the center of a hollow graphite anode that produces the majority of nanomaterials in the volume of the reactor. Furthermore, we show that arc synthesis of carbon nanotubes occurs in a sporadic fashion due to an imbalance in the rates of consumption of the anodes' graphite walls and of the filling that contains the source of the catalyst for the synthesis. Since the spectral lines of the metal catalyst are observed exclusively during the synthesis-on mode, the conditions present during synthesis-on are more optimal for production of SWCNTs than those of synthesis-off. While the arc spends significantly more time in synthesis-off mode, the majority of the nanomaterials were confirmed to be produced during the synthesis-on mode. The amount of time that is spent in each mode of the discharge was observed to be dependent on the diameter of the anode hole, with larger holes favoring the more frequent and longer synthesis-on occurrences. Additionally, the vast majority of the cathode deposit growth is observed to occur during synthesis-on mode conditions, even though the overall extent of this mode can be significantly shorter than the total arc run-time, depending on the diameter of the anode hole.

It is our opinion is that the switching of the modes can be caused by two reasons. First is the asymmetry in the rate at which the anode wall is ablated and the rate at which the filling is consumed. The powder filling is depleted faster from the top ofthe anode than its surrounding walls. Synthesis-on mode continues until thefilling level is sufficiently lower than the wall level, which causes theswitch from synthesis-on to synthesis-off. Once in synthesis-off mode, only the walls are ablated until the filling inside is reached and engaged again. Second reason may be that it is more energetically favorable for the arc to attach to solid graphite, since its resistance is lower than that of the powdered filling. It is certainly the case for measurements at low currents at room temperature. In addition, the resistance of the plasma channel increases as well, because the particles are injected into the plasma column. These two factors may make the synthesis-on mode energetically unfavorable. However, it is still unclear why the arc moves to the powdered part at all.

Given the apparent benefits of the synthesis-on mode for SWCNT synthesis, we have identified several strategies to maximize its frequency and duration. We feel this can best be achieved by addressing the ascertained cause for the observed bimodal behavior: an imbalance between the rate of wall ablation and the rate of powdered graphite/catalyst consumption. As indicated by the results presented, we have shown that the relative time spent in synthesis-on can be improved by utilizing anodes with thinner walls. Additionally, we believe that three other approaches should be investigated: (1) lower density, higher porosity graphite as the anode material, (2) supplying the metal catalyst directly, and (3)

using a solid composite anode. Lower density, higher porosity graphite ablates more quickly, bringing the wall erosion rate closer to the filling consumption rate. To circumvent the need to match the wall ablation rate to the powder consumption rate, catalyst could be supplied directly. One configuration to achieve this would be to feed powdered catalysts or a graphite/catalyst powder mixture continuously into the discharge via a gas stream or using a mechanic valve. Finally, one could employ a solid composite anode, similar to the composite pellets used for laser ablation, where a homogeneous mixture of catalyst and graphite powders is pressed into a solid electrode. By eliminating the non-uniformity of the anode in the current setup, synthesis-on should be continuous. Composite electrodes would have the added benefits of increased control over the relative ratio of catalyst to carbon in the plasma and decreased temporal fluctuations in that ratio.

The main implication of this work is that whenever one conducts an analysis of nanostructure synthesis by carbon arc using this common electrode configuration, it is necessary to differentiate between the two modes of synthesis. In the case of ex situ evaluation, carbon arc synthesis of SWCNTs has been described as having poor selectivity, forming amorphous carbon particles, SWCNHs, metal nanoparticles, and other soot in addition to SWCNTs. Based on the results herein, the observed poor selectivity could partially result from the indiscriminate sample collection method that is commonly employed. Collecting web formations from the chamber walls or stationary witness plates after arc operation has ceased precludes actual correlation of arc behavior to the materials produced. Since arc behavior and material production are bimodal (and not continuous), the “average” product is not representative of any moment during arc operation. We have shown that when the sample collection from the respective modes is isolated, the synthesis-on mode shows higher overall synthetic productivity and higher selectivity for SWCNTs over SWCNHs and amorphous carbon than does the synthesis-off mode. Given the chaotic conditions of the chamber, the selectivity we observed may actually be underestimating the actual selectivity of the synthesis-on mode. The materials produced in volume are circulating and being distributed throughout the chamber over the course of arc operation, and so a fraction of the soot collected on our witness plates during the synthesis-on mode and of the SWCNTs collected during the synthesis-off mode may be residual contamination from the opposite mode [9]. Deploying a more rapidly retractable collecting probe should allow for more accurate isolation and investigation of the products from the separate synthesis modes [10]. Most importantly, this study reveals that future in situ investigations of SWCNT growth, such as that using laser-induced incandescence, must be conducted with constant monitoring of the discharge voltage or video imaging to ensure proper correlation of the data being collected with the synthesis mode of the arc.

## Acknowledgement

The authors would like to thank to Alex Merzhevskiy for technical assistance. This work was supported by the U.S. Department of Energy, Office of Science, Basic Energy Sciences, Materials Sciences and Engineering Division.

## References

[1] S. Iijima, Helical microtubules of graphitic carbon, Nature 354 (1991) 56–58.
[2] Y. Ando, X. Zhao, Synthesis of carbon nanotubes by arc-discharge method, New Diam. Front. Carbon Technol. 16 (2006) 123–137.
[3] N. Arora, N.N. Sharma, Arc discharge synthesis of carbon nanotubes: comprehensive review, Diam. Relat. Mater. 50 (2014) 135–150.
[4] H.M. Cheng, C. Liu, Y.Y. Fan, F. Li, G. Su, L.L. He, M. Liu, Synthesis and hydrogen storage of carbon nanofibers and single wall carbon nanotubes, Z. Met. 91 (2000) 306–310.
[5] S. Iijima, T. Ichihashi, Single-shell carbon nanotubes of 1-nm diameter, Nature 363 (1993) 603.
[6] D. Bethune, C. Kiang, M. De Vries, G. Gorman, R. Savoy, J. Vasquez, R. Beyers, Cobalt-catalysed growth of carbon nanotubes with single-atomic-layer walls, Nature 363 (1993) 605.
[7] R. Das, Z. Shahnavaz, Md E. Ali, M.M. Islam, S.B.A. Hamid, Nanoscale Res. Lett. 11 (2016) 510–533.
[8] C. Journet, W.K. Maser, P. Bernier, A. Loiseau, M. Lamy de la Chapelle, S. Lefrant, P. Deniard, R. Leek, J.E. Fischerk, Large-scale production of single-walled carbon nanotubes by the electric-arc technique, Nature 388 (1997) 756.
[9] S. Yatom, J. Bak, A. Khrabry, Y. Raitses, Detection of nanoparticles in carbon arc discharge with laser-induced incandescence, Carbon 117 (2017) 154–162.
[10] X. Fang, A. Shashurin, G. Teel, M. Keidar, Determining synthesis region of the single wall carbon nanotubes in arc plasma volume, Carbon 107 (2016) 273–280.
[11] S. Gershman, Y. Raitses, Unstable behavior of anodic arc discharge for synthesis of nanomaterials, J. Phys. D. Appl. Phys. 49 (2016) 345201–345210.
[12] A. Fetterman, Y. Raitses, M. Keidar, Enhanced ablation of small anodes in a carbon nanotube arc plasma, Carbon 46 (2008) 322–326.
[13] V. Vekselman, M. Feurer, T. Huang, B. Stratton, Y. Raitses, Complex structure of the carbon arc discharge for synthesis of nanotubes, Plasma Sources Sci. Technol. 26 (2017) 065019–065030.
[14] M.S. Dresselhaus, G. Dresselhaus, R. Saito, A. Jorio, Raman spectroscopy of carbon nanotubes, Phys. Rep. 409 (2005) 47–49.
[15] M. Peña-Álvarez, E. del Corro, F. Langua, V.G. Baonza, M. Taravillo, Morphological changes in carbon nanohorns under stress: a combined Raman spectroscopy and TEM study, RSC Adv. 6 (2016) 49543–49550.
[16] A.C. Ferrari, J. Robertson, Raman spectroscopy of amorphous, nanostructures, diamond-like carbon, and nanodiamond, Philos. Trans. R. Soc. Lond. A 362 (2004) 2477–2512.